Substrate−Ligand Interactions in *Geobacillus stearothermophilus* Nitric Oxide Synthase[†]

Mariam Kabir,[‡] Jawahar Sudhamsu,[§] Brian R. Crane,[§] Syun-Ru Yeh,*[,‡] and Denis L. Rousseau*[,‡]

Department of Physiology and Biophysics, Albert Einstein College of Medicine, Bronx, New York 10461, and Department of Chemistry and Chemical Biology, Cornell University, Ithaca, New York 14853

Received August 7, 2008; Revised Manuscript Received September 17, 2008

ABSTRACT: Nitric oxide synthase (NOS) generates NO via a sequential two-step reaction [L-arginine (L-Arg) → *N*-hydroxy-L-arginine (NOHA) → L-citrulline + NO]. Each step of the reaction follows a distinct mechanism defined by the chemical environment introduced by each substrate bound to the heme active site. The dioxygen complex of the NOS enzyme from a thermophilic bacterium, *Geobacillus stearothermophilus* (gsNOS), is unusually stable; hence, it provides a unique model for the studies of the mechanistic differences between the two steps of the NOS reaction. By using CO as a structural probe, we found that gsNOS exhibits two conformations in the absence of substrate, as indicated by the presence of two sets of ν_{Fe-CO}/ν_{C-O} modes in the resonance Raman spectra. In the ν_{Fe-CO} versus ν_{C-O} inverse correlation plot, one set of data falls on the correlation line characterized by mammalian NOSs (mNOS), whereas the other set of data lies on a new correlation line defined by a bacterial NOS from *Bacillus subtilis* (bsNOS), reflecting a difference in the proximal Fe−Cys bond strength in the two conformers of gsNOS. The addition of L-Arg stabilizes the conformer associated with the mNOS correlation line, whereas NOHA stabilizes the conformer associated with the bsNOS correlation line, although both substrates introduce a positive electrostatic potential into the distal heme pocket. To assess how substrate binding affects Fe−Cys bond strength, the frequency of the Fe−Cys stretching mode of gsNOS was monitored by resonance Raman spectroscopy with 363.8 nm excitation. In the substrate-free form, the Fe−Cys stretching mode was detected at 342.5 cm^{-1}, similar to that of bsNOS. The binding of L-Arg and NOHA brings about a small decrease and increase in the Fe−Cys stretching frequency, respectively. The implication of these unique structural features with respect to the oxygen chemistry of NOS is discussed.

Mammalian nitric oxide synthase (mNOS)[1] produces NO via a sequential two-step reaction (*1*). In the first step of the reaction, L-Arg is oxidized to *N*-hydroxy-L-arginine (NOHA), with the consumption of two electrons and one molecule of oxygen. In the second step, NOHA is further oxidized to L-citrulline and NO, by using an additional electron and another molecule of oxygen as illustrated in Scheme 1. The three major isoforms of mNOS present in macrophages

Scheme 1

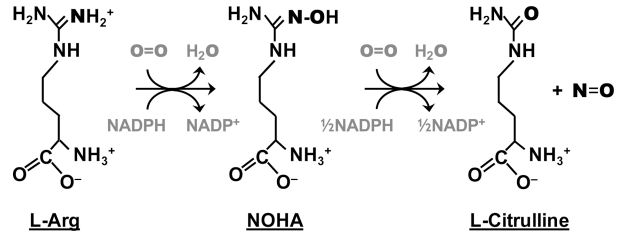

(iNOS), endothelial cells (eNOS), and neuronal tissues (nNOS) produce NO that functions as a cytotoxic agent, a vasodilator, and a neurotransmitter, respectively. All three isoforms of mNOS consist of a reductase domain with NADPH, FAD, and FMN binding sites, and an oxygenase domain, containing tetrahydrobiopterin (H4B), heme, and the substrate binding sites (*1*). The mNOS enzymes function as a dimer, and during the reaction, an electron travels from the NADPH to FAD to FMN in the reductase domain of one subunit, culminating in the heme iron of the oxygenase domain of the other subunit, where the oxygen reaction takes place (*2*). Calcium/calmodulin binding enables electron transfer between the two domains (*3*).

Although the full-length mNOS enzymes have not been crystallized, the structures of the oxygenase domains of all three mammalian isoforms ($mNOS_{oxy}$) have been determined and found to be nearly identical (*4*−*9*). It is important to

[†] This work was supported by grants from the National Institutes of Health (NIH) (GM054806 to D.L.R.) and from the National Science Foundation (CHE-0749997 to B.R.C.). M.K. is supported by the Medical Scientist Training Program at the Albert Einstein College of Medicine (NIH Grant GM08572).

* To whom correspondence should be addressed. S.-R.Y.: e-mail, syeh@aecom.yu.edu; telephone, (718) 430-4234; fax, (718) 430-4230. D.R.: e-mail, rousseau@aecom.yu.edu; telephone, (718) 430-4264; fax, (718) 430-8808.

[‡] Albert Einstein College of Medicine.

[§] Cornell University.

[1] Abbreviations: 5C and 6C, five- and six-coordinate hemes, respectively; H4B, (6*R*)-5,6,7,8-tetrahydro-L-biopterin; NOHA, *N*-hydroxy-L-arginine; NOS, nitric oxide synthase; NOS_{oxy}, oxygenase domain of nitric oxide synthase; eNOS, iNOS, and nNOS, endothelial, inducible, and neural mammalian nitric oxide synthases, respectively; mNOS, mammalian nitric oxide synthase; bsNOS, gsNOS, and saNOS, nitric oxide synthases from the bacteria *Bacillus subtilis*, *Geobacillus stearothermophilus*, and *Staphylococcus aureous*, respectively; ν_{Fe-CO}, ν_{C-O}, and ν_{Fe-Cys}, Fe−CO, C−O and Fe−Cys stretching modes, respectively; δ_{Fe-C-O}, Fe−C−O bending mode; PDB, Protein Data Bank.

10.1021/bi801491e CCC: $40.75
Published on Web 10/29/2008

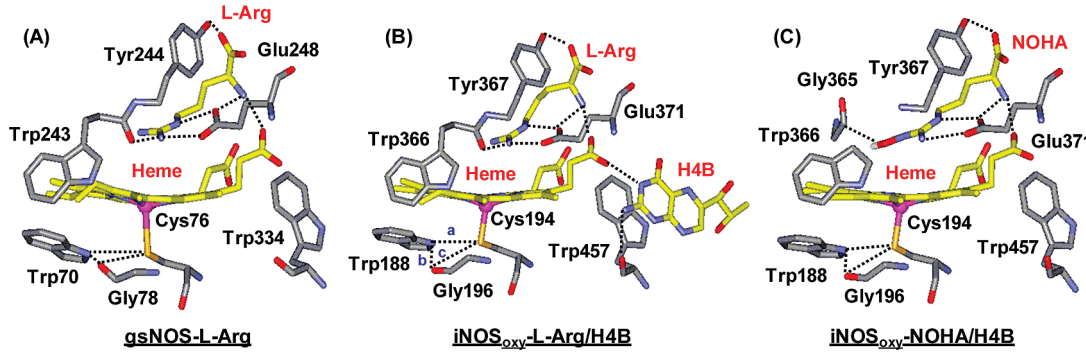

FIGURE 1: Catalytic site of (A) L-Arg-bound gsNOS (PDB entry 2FLQ), (B) L-Arg-bound $iNOS_{oxy}$ (PDB entry 1NOD), and (C) NOHA-bound $iNOS_{oxy}$ (PDB entry 1DWX). In panels B and C, H4B is also present in the crystal structures, but not shown in panel C for the sake of clarity. The H-bonding interactions are represented by the dashed lines. The distances indicated in panel B by a, b, and c on the proximal side of each heme are listed in Table 2.

Table 1: Various Heme Ligand-Related Vibrational Frequencies (cm^{-1}) in gsNOS As Compared to Those of Other NOSs[a]

NOS		ν_{Fe-CO}	ν_{C-O}	δ_{Fe-C-O}	ν_{Fe-Cys}	ref
gsNOS	S-free ± H4B	483 (m), 501 (m)	1952 (m), 1929 (m)	562	342.5	this work
	L-Arg ± H4B	505 (s), 517 (w)	1923	566	342.1	
	NOHA ± H4B	493 (s), 513 (w)	1929	561	343.3	
bsNOS	S-free	485 (m), 499 (m)	1943 (s), 1914 (w)	564		*25*
	L-Arg	502	1910	568		
	H4B	487 (m), 501 (s)	1944 (m), 1933 (m), 1917 (m)			
	L-Arg ± H4B	501	1915	567	342	
saNOS	S-free	482 (m), 497 (m)	1949 (m), 1930 (m)	560		*27*
	L-Arg ± H4B	504	1917	566		
$iNOS_{oxy}$	S-free ± H4B	482 (m), 502 (m)	1945 (broad)	562		*32*, *33*, *38*
	L-Arg ± H4B	482 (w), 502 (m), 512 (s)	1907	569	337	*25*, *32*, *33*, *38*
	NOHA ± H4B	482 (m), 500 (s), 512 (w)	1930 (m), 1904 (w)	562		*32*, *33*, *38*
$nNOS_{oxy}$	S-free ± H4B	489 (s), 501 (w), 514 (w)		562		*32*, *33*, *50*
	L-Arg ± H4B	489 (m), 502 (m), 514 (m)	1932	565		
	NOHA ± H4B	490 (m), 501 (m), 514 (w)		562		

[a] The relative intensities of the multiple ν_{Fe-CO} and ν_{C-O} modes are indicated as w (weak), m (medium), or s (strong).

Table 2: Distances between the Three Critical Proximal Amino Acids in the Crystallographic Structure of Each Subunit of Various NOSs[a]

		subunit A			subunit B		
NOS	PDB	$S_{Cys}-N_{Trp}$	$N_{Trp}-O_{Gly}$	$O_{Gly}-S_{Cys}$	$S_{Cys}-N_{Trp}$	$N_{Trp}-O_{Gly}$	$O_{Gly}-S_{Cys}$
$eNOS_{oxy}$ (+Arg)	4NSE	3.38	4.37	4.81	3.32	4.19	4.82
$nNOS_{oxy}$ (+Arg+H4B)	1OM4	3.44	4.44	4.85	3.49	4.31	4.86
$iNOS_{oxy}$ (+Arg+H4B)	1NOD	3.22	4.71	5.08	3.23	4.39	4.83
$iNOS_{oxy}$ (+NOHA+H4B)	1DWX	3.15	4.69	5.02	3.14	4.41	4.74
saNOS	1MJT	3.29	3.97	4.46	3.36	4.03	4.45
bsNOS	2AMO	3.74	4.31	4.86	3.40	3.77	4.49
bsNOS (+Arg+THF)	1M7V	3.47	4.04	4.80			
bsNOS (+NOHA+THF)	1M7Z	3.48	4.01	4.80			
gsNOS	2FLQ	3.73	3.07	3.89	3.74	3.61	3.90

[a] The distances, $S_{Cys}-N_{Trp}$, $N_{Trp}-O_{Gly}$, and $O_{Gly}-S_{Cys}$, are defined as a, b, and c, respectively, in Figure 1B, which correspond to the distances between the sulfur atom of the proximal cysteine and the nitrogen atom of the nearby tryptophan (a), the nitrogen atom of the tryptophan and the backbone oxygen atom of the nearby glycine (b), and the oxygen atom of the glycine and the sulfur atom of the proximal cysteine (c).

note that the oxygenase domain of mNOS ($mNOS_{oxy}$) is fully functional in the presence of the substrate and cofactor in vitro, when an electron source is available (*10*). As illustrated in panels B and C of Figure 1, using the crystal structures of $iNOS_{oxy}$ as an example, the substrate binds directly over the heme iron, consistent with the prediction made by a variety of spectroscopic studies (*11*−*15*). The binding is stabilized by a H-bonding network involving Glu371, Trp366, and Tyr367, as well as one of the two heme propionate groups and H4B. As a member of the P450 family of enzymes, the heme iron in NOS is coordinated by a cysteine residue (Cys194 in iNOS) as the proximal ligand. Nonetheless, distinct from P450, in which the proximal cysteine thiolate ligand is H-bonded to three backbone amino groups, the proximal cysteine ligand of mNOS accepts a H-bond from a nearby Trp residue side chain (Trp188 in iNOS) (*16*−*20*), in addition to two H-bonds from backbone amino groups. The Trp−Cys H-bond is believed to be important in regulating the electron density on the heme iron for oxygen chemistry (*16*−*19, 21*).

In addition to mammals, genes encoding NOS-like enzymes have been found in several other organisms, including bacteria. Seven bacterial NOSs, including those from *Streptomyces turgidiscabies* (*22*), *Nocardia* sp. (*23*), *Deinococcus radiodurans* (*24*), *Bacillus subtilis* (bsNOS) (*25*), *Bacillus anthracis* (*26*), *Staphylococcus aureous* (saNOS) (*27*), and *Geobacillus stearothermophilus* (gsNOS) (*28*), have been expressed and partially characterized. Among them, bsNOS (*29*), saNOS (*30*), and gsNOS (*28*) have been crystallized. The structures of the three bacterial NOSs are very similar.

They exhibit characteristics resembling those of $mNOS_{oxy}$ (see panels A and B of Figure 1), except that the bacterial NOSs lack a portion of the cofactor binding site, as well as the N-terminal hook, which links the two subunits of the dimer together in nMOS (*5*) and the associated Zn-binding site. Although these two structural features have been recognized to be important in the formation of the dimer interface in mNOS (*31*), their absence in bacterial NOS does not seem to compromise their ability to form dimers. On the contrary, the dimeric interactions in the bacterial NOS are as strong as those of their mammalian counterparts (*29*).

Although the overall crystallographic structures of the bacterial NOSs and $mNOS_{oxy}$ are similar, distinct solution structural properties have been revealed by a variety of spectroscopic studies as summarized by Salard et al. (*26*). For example, on the basis of optical absorption measurements (*26*), the heme iron in the substrate and cofactor-free ferric derivative of saNOS has either a six-coordinate (6C) low-spin or a high-spin/low-spin mixed electronic configuration, like that observed in the mNOSs, indicating a water molecule is coordinated to the heme iron on the distal side, whereas that in bsNOS is a five-coordinate (5C) high-spin form, suggesting that the water molecule is destabilized in the distal ligand binding site. On the other hand, resonance Raman studies of the CO adducts of both bsNOS (*27*) and saNOS (*25*) revealed two Fe−CO stretching modes ($\nu_{Fe\text{-}CO}$) in the 480−500 cm^{-1} region, corresponding to two possible conformers of the Fe−CO moiety. As in the bacterial enzymes, in iNOS two conformers were detected (*32*), whereas in nNOS, three conformers were reported (*32, 33*). In addition, L-Arg binding in the bacterial NOSs causes the merging of the two ν_{Fe-CO} modes into a single mode at ∼502−504 cm^{-1}, similar to the frequency observed in nNOS, but distinct from that of iNOS and eNOS (in which the mode is located at ∼512 cm^{-1}) (*14*). In contrast to bsNOS and saNOS, until now no resonance Raman studies have been reported for the NOS from *G. stearothermophilus*.

G. stearothermophilus is a thermophilic bacterium found in warm compost. It lives optimally between 43 and 75 °C, and as such, the rate of turnover of gsNOS is slower at room temperature as compared to those of other members of the NOS family (*28*). Furthermore, the decay rate of the primary dioxygen-bound intermediate of gsNOS has been found to be ∼10-fold slower than that of other NOS enzymes (*28*). Although some relatively minor structural differences in the distal heme pocket of gsNOS have been noted as compared to $mNOS_{oxy}$ (*28*), the heme active sites of the NOSs are nearly superimposable (see Figure 1A,B) (*28*), and there are no obvious structural features that may account for the enhanced stability of the dioxygen complex of gsNOS.

The understanding of the catalytic mechanism of the NOS enzymes has been hampered by the fact that no oxygen-containing intermediates other than the primary dioxygen complex have been well-characterized during the reaction cycle. Nonetheless, on the basis of various spectroscopic studies (*32, 34−37*), it is generally believed the first step of the NOS reaction (L-Arg → NOHA) follows the P450 type of mechanism, in which the active oxygen species is a Compound I-type ferryl intermediate (*32, 34, 36*), whereas the second step of the reaction (NOHA → L-citrulline + NO) follows the heme oxygenase type of chemistry, where the active oxygen species is a peroxyl intermediate (*32, 37*). The difference in the catalytic mechanisms of the two steps of the NOS reaction indicates that L-Arg and NOHA interact differently with the heme-bound dioxygen in the catalytic site of NOS, thereby dictating the mechanism by which the oxygen chemistry proceeds. The nature of the interaction between the substrates and heme-bound ligand in NOS may be studied by using CO as a structural probe. With this approach, the isoform-specific substrate−ligand interactions in $mNOS_{oxy}$ have been identified (*14*) and the differing interactions between the substrates and the catalytic pockets have been examined (*13, 21, 32, 38*). In this work, optical absorption and resonance Raman spectroscopies were used to study various derivatives of gsNOS in the absence and presence of substrate (either L-Arg or NOHA) and cofactor (H4B). The results are compared to those of mNOSs as well as other bacterial NOSs and discussed in the context of oxygen chemistry in NOS.

MATERIALS AND METHODS

(6*R*)-5,6,7,8-Tetrahydro-L-biopterin was purchased from Alexis Biochemicals (San Diego, CA). All other chemicals were purchased from Sigma. The isotopically labeled gas, $^{13}C^{16}O$, was supplied by Icon (Mount Marion, NY). The naturally abundant gases, Ar and CO, were obtained from Tech Air (White Plains, NY).

The gsNOS samples were purified in the absence of L-Arg and H4B as reported previously (*28*). The purified gsNOS was kept in Tris buffer (50 mM) in the presence of 150 mM NaCl at pH 7.5 and stored in liquid nitrogen until it was used. To generate the L-Arg and NOHA and/or H4B-bound derivatives, L-Arg or NOHA and/or H4B were added to the enzyme in 100−150- and 3−5-fold excesses with respect to the heme, respectively, and incubated at 4 °C for ∼18 h. The binding of L-Arg and NOHA was confirmed by monitoring the optical absorption change. Although the addition of H4B did not result in any changes in the optical spectrum, the binding of H4B, at a 3−5-fold excess, was confirmed by a large change in both the kinetics and thermodynamics of the decay of the primary oxy intermediate of gsNOS in stopped-flow optical absorption measurements (unpublished data). To prepare the deoxy derivatives, the protein sample was first purged with Ar gas in a septum-sealed anaerobic cell and reduced with sodium dithionite introduced via a gastight syringe. To prepare the CO derivatives, 500 μL of 1 atm of CO was injected into the deoxy samples via a gastight syringe. The protein concentration used for the optical absorption and resonance Raman studies was ∼50 μM.

The optical absorption spectra were recorded with a Shimadzu UV2100U spectrophotometer. Resonance Raman spectra were obtained by using 441.6 nm excitation from a He−Cd laser (Liconix, Santa Clara, CA) for spectra of the CO-bound adducts and 363.8 nm excitation from an argon ion laser (Spectra-Physics, Beamlok 2080) for spectra of the ferric form of the enzyme to enhance the Fe−Cys stretching mode. The incident laser power on the sample was kept under 3 mW. The cylindrical sample cell was rotated at ∼6000 rpm during the spectral acquisition to avoid photodamage to the sample. The scattered light was collected and focused onto an entrance slit (100 μm) of a 1.25 m SPEX spectrophotometer (Jobin Yvon, Edison, NJ) and subsequently

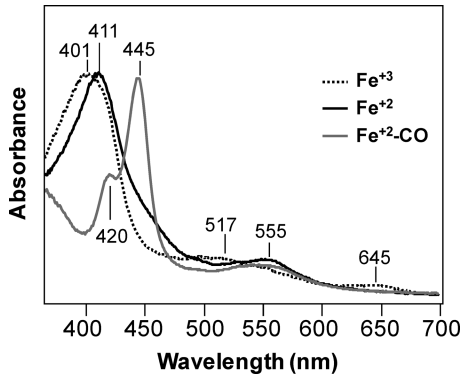

FIGURE 2: Optical absorption spectra of the ferric (dotted line), ferrous (solid black line), and CO-bound ferrous (solid gray line) forms of gsNOS in the absence of substrates and cofactor.

detected with a liquid nitrogen-cooled CCD (Roper Scientific, Princeton, NJ). All of the resonance Raman spectra were frequency-calibrated by using spectral lines from indene, except for those in the 1800−2000 cm^{-1} spectral region, where an acetone/ferricyanide combination was used instead. Cosmic ray artifacts were removed from the spectra by using a routine in the Winspec spectral acquisition software (Roper Scientific). Most of the data were integrated for ∼30 min. Longer integration times of 180 and 360 min were used to improve the signal-to-noise ratio for the Fe−Cys and C−O stretching frequency regions. All measurements were taken at room temperature. Optical absorption spectra were obtained before and after each resonance Raman measurement to ensure the integrity of the enzyme.

RESULTS

Optical Absorption Spectroscopic Studies. Figure 2 shows the optical absorption spectra of gsNOS in the absence of substrate and cofactor. The oxidized enzyme has a broad Soret transition at 401 nm, characteristic of a five-coordinate high-spin electronic configuration. Upon reduction, the Soret maximum shifts to ∼411 nm, again indicating a five-coordinate high-spin electronic configuration, similar to that seen in other reduced NOSs (*21*). The addition of CO to the ferrous enzyme causes a further shift of the Soret band to 445 nm, typical for a six-coordinate low-spin configuration of a CO-bound heme with coordination of a thiolate ligand on the proximal side. The shoulder at ∼420 nm, typical of histidine-coordinated CO complexes, is attributed to the presence of a small amount of the inactive form of the enzyme commonly observable in mNOSs (*12*).

The addition of L-Arg or NOHA to the ferric enzyme causes the Soret maximum to shift from 401 to 397 nm and the Soret band to be more symmetric, whereas the addition of H4B does not introduce any appreciable spectral shift (Figure 1S of the Supporting Information). Also, both substrates cause the Soret maximum of ferrous gsNOS to shift from 411 to 414 nm. As in the case of ferric gsNOS, the addition of H4B does not bring about additional changes. On the other hand, the addition of substrate and/or cofactor to CO-bound gsNOS reduces the intensity of the 420 nm band significantly without affecting the main 445 nm band, indicating the stabilization of the gsNOS structure by the binding of substrate and/or cofactor.

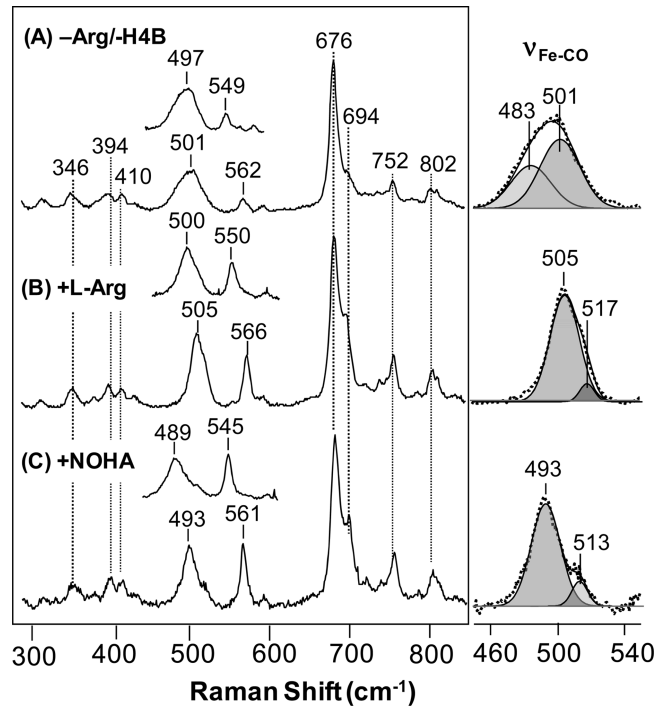

FIGURE 3: Resonance Raman spectra of $^{12}C^{16}O$-bound gsNOS in the absence of substrates and cofactor (A), in the presence of L-arginine (B), and in the presence of NOHA (C). The insets above each spectrum show the spectra of the same derivatives obtained with $^{13}C^{16}O$-bound gsNOS. The right panel shows the best fit of each Fe−CO stretching mode with two Gaussian curves as indicated by the shaded areas. All the parameters were allowed to free-float in the fitting routine. The dotted lines are the experimental data, and the solid lines are the fits.

Resonance Raman Spectroscopic Studies of the CO-Bound Adducts. The CO-bound form of the enzyme was studied with resonance Raman spectroscopy, by using 441.6 nm excitation to probe selectively the active species associated with the Soret maximum at 445 nm. Figure 3 shows the low-frequency region of the resonance Raman spectra of the CO-bound gsNOS in the absence or presence of substrate (either L-Arg or NOHA). These spectra are not affected by the addition of H4B, independent of the presence or absence of substrates (Figure 2S of the Supporting Information).

In the absence of substrate, the broad line at ∼501 cm^{-1} (left panel in Figure 3) is assigned as the Fe−CO stretching mode (ν_{Fe-CO}), which can be fitted with two Gaussian curves with peak maxima at 483 and 501 cm^{-1} (see the right panel). The small line at 562 cm^{-1} is assigned to the Fe−C−O bending mode (δ_{Fe-C-O}). The assignments of these vibrational modes were confirmed by the isotope substitution of $^{12}C^{16}O$ with $^{13}C^{16}O$ (Figure 3 and Figure 2S of the Supporting Information). In the high-frequency region of the spectra (Figure 4), two overlapping lines at 1929 and 1952 cm^{-1} are identified as the C−O stretching modes (ν_{C-O}). These data demonstrate that there are two different conformations of the Fe−CO moiety in the absence of added substrates, as reported for other members of the enzyme family (*11, 13, 14, 25, 27, 33, 38, 39*).

In general, when CO binds to heme proteins, it donates electron density to the heme iron via a σ-bond to the empty d_{z^2} orbital of the iron, which in turn donates electron density back to the π^* orbital of the CO. Because of the so-called "π-back-bonding" effect, CO-bound heme proteins can exist in two extreme structures:

$$Fe^{\delta-}-C\equiv O^{\delta+}(I) \leftrightarrow Fe=C=O(II) \quad (1)$$

When the distal environment is positively charged, structure II is favored over structure I. Consequently, the Fe−CO bond strength increases, resulting in an increase in the $\nu_{Fe\text{-}CO}$ stretching frequency, and the C−O bond strength decreases, resulting in a decrease in the ν_{C-O} stretching frequency (*40*−*42*). On this basis, the ν_{Fe-CO} frequency is inversely correlated with the ν_{C-O} frequency as illustrated in Figure 5 with the position on a given curve determined by the charge distribution in the distal heme environment. This relationship has made CO a very important probe of the distal pocket in heme proteins.

In addition to its sensitivity to the distal environment, the position of the specific ν_{Fe-CO} versus ν_{C-O} correlation line depends on the strength of the proximal ligand bond, which determines the degree of electron donation to the heme iron, thereby modulating the π-bonding effect (*40*−*42*). As such, the correlation line associated with heme proteins with histidine as the proximal ligand, such as hemoglobin and myoglobin, lies above that associated with heme proteins with thiolate as the proximal ligand, such as P450 (Figure 5). Interestingly, the mNOS data points fall between those two correlation lines, suggesting a proximal thiolate−iron bond (Fe−Cys) weaker than that in the P450 enzymes. The weaker Fe−Cys bond in mNOS is believed to be a result of the H-bond between the proximal cysteine and a nearby Trp residue (see Figure 1), which withdraws electron density from the Fe−Cys bond, thereby strengthening the Fe−CO σ-bond (*13*, *42*, *43*). Recently, Santolini et al. reported that the ν_{Fe-CO} versus ν_{C-O} correlation line of bsNOS (*25*) falls between the mNOS and P450 lines (Figure 5), suggesting a

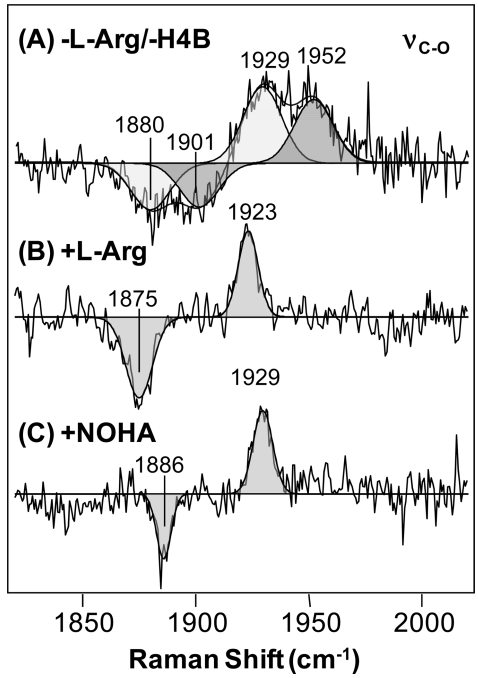

FIGURE 4: Resonance Raman isotope difference spectra ($^{12}C^{16}O$ − $^{13}C^{16}O$) for the C−O stretching modes of CO-bound gsNOS in the absence of substrates and cofactor (A), in the presence of L-Arg (B), and in the presence of NOHA (C). In A, each difference spectrum was fitted with two Gaussian curves for the positive bands and two Gaussian curves for the negative bands, with procedures described in the legend of Figure 3. As the signal in this region is very weak, the difference spectra, instead of the original spectra, were analyzed.

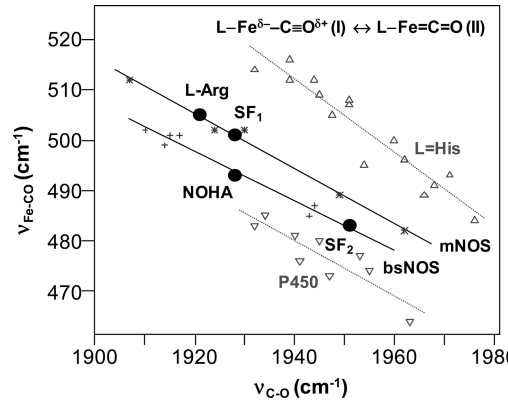

FIGURE 5: ν_{C-O}−ν_{Fe-CO} inverse correlation plot of the CO derivatives of heme proteins with a proximal ligand of histidine (△), the mNOS enzyme family (∗), the bsNOS enzyme (+), and the P450 enzyme family (▽). The data indicated as SF_1 and SF_2 are those associated with the substrate-free gsNOS. The data indicated as L-Arg and NOHA are those associated with L-Arg- and NOHA-bound gsNOS, respectively. The data points for gsNOS (●) fall on two different correlation lines. All points other than those from gsNOS were taken from prior reports (*40*−*42*).

Fe−Cys bond that is stronger than that in mNOSs but weaker than that in P450s. This conclusion is consistent with the ∼5 cm^{-1} higher Fe−Cys stretching frequency (ν_{Fe-Cys}) of bsNOS with respect to that of mNOS (Table 1).

The Raman data of the substrate-free (SF) gsNOS shown in Figures 3 and 4 indicate the presence of two sets of ν_{Fe-CO}/ν_{C-O} modes, one at 501/1929 cm^{-1} and the other at 483/1952 cm^{-1} (denoted as SF_1 and SF_2, respectively, in Figure 5). Surprisingly, the SF_1 data point lies on the mNOS correlation line, whereas the SF_2 point lies on the bsNOS correlation line (see the black circles in Figure 5). The data suggest that, in the absence of substrate and cofactor, the two conformers of gsNOS exhibit distinct proximal as well as distal environments. This behavior is unique among the NOS family of enzymes; as one can see in Figure 5, all the data associated with mNOS or bsNOS fall on the same correlation line, despite the fact that conformational heterogeneity is also present in these enzymes (*21*).

In the presence of L-Arg, the ν_{Fe-CO} mode is sharpened and shifts to 505 cm^{-1}. Curve fitting of the ν_{Fe-CO} mode revealed the presence of a weak line at 517 cm^{-1}, which is presumed to be a minor conformation of the complex. The ν_{C-O} mode associated with the major conformer is observed at 1923 cm^{-1}, whereas that associated with the minor conformer is too weak to be detected (Figure 4) and has not been analyzed further. The δ_{Fe-C-O} mode, on the other hand, shifts from 562 to 566 cm^{-1} with a significantly enhanced intensity, characteristic of a bent conformation of the Fe−C−O moiety. The ν_{Fe-CO}/ν_{C-O} data point associated with the L-Arg-bound enzyme lies on the mNOS correlation line and shifts higher toward the left corner with respect to the SF_1 conformer of the substrate-free enzyme (Figure 5). The data indicate that the guanidinium group of the L-Arg is in the proximity of the heme-bound CO, thereby introducing a positive electrostatic potential to the environment of the CO and forcing the Fe−C−O moiety to adopt a bent conformation.

In the presence of NOHA, the ν_{Fe-CO} mode is detected at 493 cm^{-1} (Figure 3). Curve fitting of the ν_{Fe-CO} band revealed the presence of a weak line at 513 cm^{-1}. The ν_{C-O} mode associated with the major conformer is observed at

1929 cm^{-1}, while that associated with the minor conformer is not visible (Figure 4). Again, no additional analysis of the minor conformation was undertaken. The δ_{Fe-C-O} mode slightly shifts to 561 cm^{-1} and is significantly enhanced, indicating a bent Fe−C−O moiety. Intriguingly, the ν_{Fe-CO}/ν_{C-O} data point associated with the NOHA-bound enzyme falls on the bsNOS correlation line and shifts higher toward the left corner with respect to the SF_2 conformer of the substrate-free enzyme (Figure 5), again indicating that NOHA introduces a positive electrostatic potential into the surroundings of the CO.

As summarized in Table 1 and Figure 5, the structural perturbations introduced by substrate binding into the various members of the NOS family of enzymes are quite disparate, manifesting the possible structural features that may account for the wide spectrum of the activities associated with the various derivatives of the enzymes. The significantly enhanced δ_{Fe-C-O} in gsNOS induced by substrate binding is unique compared to that of mNOS, suggesting a congested ligand binding site in gsNOS in the presence of substrates. Taken together, the data suggest that the substrate-free gsNOS exhibits structural flexibility, allowing for the coexistence of two conformers, with distinct proximal Fe−Cys bond strengths and distal electrostatic potentials. The binding of the substrates to gsNOS imposes structural constraints on the protein matrix, forcing the Fe−C−O moiety to adopt a bent structure and locking the enzyme in conformations with proximal Fe−Cys bond properties similar to those of mNOS and bsNOS for the L-Arg- and NOHA-bound enzyme, respectively.

Resonance Raman Spectroscopic Studies of the Iron−Sulfur (Fe−Cys) Stretching Mode. To determine the possible role of Fe−Cys bond strength in modulating the chemical properties of the Fe−C−O moiety, we measured the Fe−Cys stretching mode (ν_{Fe-Cys}) of gsNOS in the absence or presence of L-Arg or NOHA, with and without H4B. To probe the ν_{Fe-Cys} frequency of gsNOS, 363.8 nm excitation and the ferric enzyme were used for the resonance Raman measurements, as the ν_{Fe-Cys} mode of P450 and other NOS systems is only selectively enhanced in the ferric oxidation state with a five-coordinate high-spin electronic configuration (*25, 44−47*).

A strong line in the 342−344 cm^{-1} region was identified under all the conditions that were examined, as shown in Figure 6. Curve fitting analysis of the data obtained in the absence of substrate shows a major line located at 342.5 cm^{-1} and two minor lines at 350 and 375 cm^{-1} assigned as intrinsic porphyrin modes. The 342.5 cm^{-1} line is assigned as the Fe−Cys stretching mode, as its intensity is dramatically enhanced with the 363.8 nm excitation as compared to the Soret excitation. Interestingly, the ν_{Fe-Cys} frequency is sensitive to substrate binding (Figure 6), but insensitive to H4B binding (Figure 3S of the Supporting Information). The ν_{Fe-Cys} frequency shifts from 342.5 cm^{-1} to 342.1 and 343.3 cm^{-1} for the L-Arg- and NOHA-bound enzyme, respectively. Although the shifts are small, they are confirmed by the difference spectrum shown in Figure 6, where the peak and trough correlate with the ν_{Fe-Cys} lines of the NOHA- and L-Arg-bound enzyme, respectively. The ν_{Fe-Cys} frequencies of gsNOS are similar to that of bsNOS (~342 cm^{-1}), lower than that of P450 (~351 cm^{-1}) (*44−46*), but higher than that of mNOS (~337 cm^{-1}) (*25, 47*).

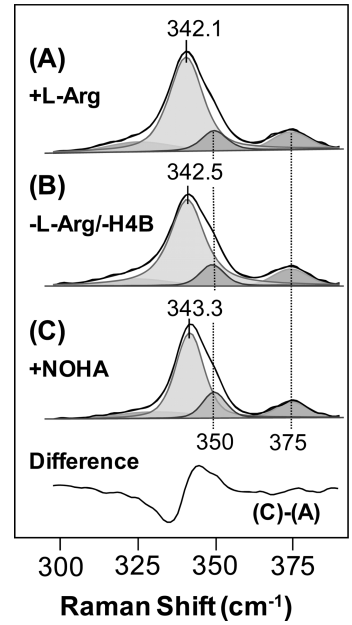

FIGURE 6: Fe−Cys stretching modes of the various derivatives of gsNOS. The bottom trace shows the difference spectrum of C minus A. Each mode was fitted with a Gaussian/Lorentzian mixture, with all the parameters free-floating. The lines at 350 and 375 cm^{-1} are assigned as porphyrin modes.

DISCUSSION

The data reported here demonstrate that the substrate−ligand interactions in gsNOS are quite distinct from those of the other members of the NOS family. The coexistence of two conformers of the CO complex that lie on differing ν_{Fe-CO}−ν_{C-O} correlation lines is unprecedented. It demonstrates a great deal of plasticity in the protein matrix that has functional implications. To gain an understanding of the origin of these features, we consider the relationship between the strength of the Fe−Cys bond and the position of the ν_{Fe-CO} versus ν_{C-O} correlation curves as well as the factors that regulate the strength of the bond.

Relationship between the Proximal Fe−Cys Bond Strength and the Distal Fe−C−O Bond Strengths. To understand how the proximal Fe−Cys bond strength affects the chemical properties of the distal Fe−C−O moiety in a quantitative fashion, the offset of the ν_{Fe-CO} versus ν_{C-O} correlation line shown in Figure 5, as estimated by the ν_{Fe-CO} value at the ν_{C-O} = 1945 cm^{-1} point, is plotted against the ν_{Fe-Cys} frequency in Figure 7. It was found that all the data points, except those associated with the SF_1 conformer of the substrate-free gsNOS and the L-Arg-bound gsNOS, fall on a linear line. The linear relationship confirms that the displacement of the ν_{Fe-CO}−ν_{C-O} correlation lines shown in Figure 5 is proportional to the strength of the Fe−Cys bond.

One plausible explanation for the deviation of the SF_1 and L-Arg points from the line shown in Figure 7 is that the Fe−Cys bond strength measured in the ferric state does not necessarily reflect that associated with the CO-bound ferrous state. For example, the sensitivity of the proximal Fe−Cys bond strength to the oxidation state of the heme iron in heme proteins has been reported for the P450 and CPO enzymes (*48*), in which the Fe−Cys bond lengths are 2.23 and 2.30 Å, respectively, in the ferric high-spin states, whereas they are 2.37 Å in the ferrous oxy complexes of both of the enzymes. It is conceivable that in the ferric form of gsNOS,

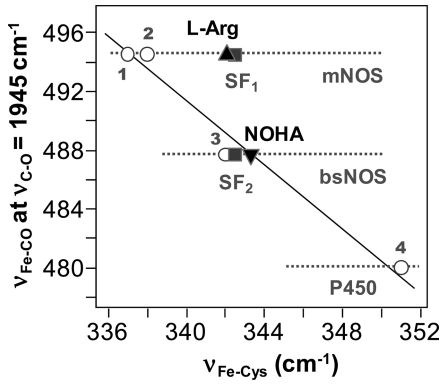

FIGURE 7: Plot of the offset of the $\nu_{C-O}-\nu_{Fe-CO}$ inverse correlation line shown in Figure 5 as a function of the ν_{Fe-Cys} frequency. The offsets of the inverse correlation lines are taken from the *y*-intercept in Figure 5, defined by the ν_{Fe-CO} frequency at a ν_{C-O} of 1945 cm^{-1}. Data points 1 and 2 are from mNOS (*25, 47*), while data points 3 and 4 are from bsNOS (*25*) and P450 in the absence of putaredoxin (*45, 51*), respectively. The black squares, indicated as SF_1 and SF_2, are associated with the two data points of the substrate-free gsNOS. The up and down triangles are associated with L-Arg- and NOHA-bound gsNOS, respectively.

the structure is locked into a conformation with a relatively strong Fe−Cys bond strength independent of the presence of the substrate, giving the relatively high frequency of the Fe−Cys mode for all of the ferric complexes. However, in the CO complexes, this conformational restraint is relieved, revealing distinct substrate-dependent Fe−Cys bond strengths. Consequently, the data indicate that in the SF_1 and L-Arg-bound CO complexes of gsNOS, the Fe−Cys bond strengths are overestimated by the resonance Raman measurements of the 5C ferric states shown in Figure 6.

Structural Features Controlling the Proximal Fe−Cys Bond Strength. As listed in Table 1, the Fe−Cys bond strengths of the ferric NOS are in the following order: $iNOS_{oxy}$ < gsNOS ∼ bsNOS. In the crystallographic structure of the ferric form of gsNOS [PDB entry 2FLQ (*28*) (Figure 1A)], the proximal Cys76 ligand accepts a H-bond from a nearby Trp70. The H-bond between Cys76 and Trp70 presumably modulates the donation of electron density from Cys76 to the heme iron, thereby regulating the bond length and/or bond strength of the Fe−Cys moiety. Similar interactions are present in mNOS as illustrated in panels B and C of Figure 1 (using iNOS as an example). The equivalent Trp residue in nNOS has been demonstrated to play a critical role in controlling the NO binding properties of the enzyme, and consequently in regulating the NO feedback inhibition mechanism (*16*−*20*). The Cys−Trp distance is modulated by additional H-bonding interaction(s) with the backbone carbonyl group of a nearby residue (see Gly78 and Gly196 in gsNOS and iNOS, respectively). As listed in Table 2, the Cys−Trp distances are ∼3.74 and 3.22 Å in gsNOS and $iNOS_{oxy}$, respectively. The shorter Trp−Gly distance (3.07 or 3.61 Å vs 4.71 Å) is associated with the longer Cys−Trp distance in gsNOS, resulting in a weaker Trp−Cys H-bond, and consequently a shorter Fe−Cys bond (which cannot be accurately determined due to the limited resolution of the crystal structure), accounting for the higher ν_{Fe-Cys} frequency in gsNOS reported in this work.

The ν_{Fe-Cys} frequency of bsNOS, on the other hand, is similar to that of gsNOS (Table 1). However, two different Trp−Cys distances, 3.74 and 3.39 Å, were observed in the two subunits of the loose dimeric bsNOS enzyme in the absence of substrate and cofactor (PDB entry 2AMO) (*49*). The longer distance is identical to that observed in gsNOS, suggesting that the subunit structure associated with the Trp−Cys distance of 3.74 Å is the energy minimum state of bsNOS in free solution, and that the coexistence of the two conformations may be a result of crystal packing. In the presence of THF and L-Arg (or NOHA), both subunits are identical, with Trp−Cys distances of 3.47 and 3.48 Å (*29*).

As shown in Figure 5, L-Arg and NOHA binding in gsNOS induces opposite effects: the former weakens the Fe−Cys bond, whereas the latter strengthens it. As the crystal structure of NOHA-bound gsNOS is not available, to improve our understanding of how the distal substrate−protein interaction affects the proximal Fe−Cys bond strength, we compare the crystal structure of L-Arg-bound $iNOS_{oxy}$ (Figure 1B) to that of NOHA-bound $iNOS_{oxy}$ (Figure 1C). In the NOHA-bound structure, the terminal oxygen atom of the NOHA is in the proximity of a porphyrin nitrogen atom of the heme; in addition, it forms a H-bond with the backbone amine group of Gly365. These interactions, which are absent in the L-Arg-bound structure, may introduce heme distortion, which in turn may affect the position of Trp188. As the side chain of Trp188 engages in π-stacking with the heme, the change in its positioning would affect its H-bonding interaction with Cys194 and thus the Fe−Cys bond strength. This hypothesis remains to be tested by additional crystallographic studies of NOHA-bound gsNOS.

Implications in the Oxygen Chemistry of NOS. All the CO derivatives of mNOS exhibit multiple conformations in the absence of substrates and cofactor, indicating a significant degree of conformational heterogeneity (*13, 14, 32, 38*). Substrate binding in these enzymes reduces the level of conformational freedom by affecting only the local interactions in the distal heme pocket, without perturbing the proximal heme environment, as indicated by the fact that all the $\nu_{Fe-CO}-\nu_{C-O}$ data of the substrate-free and -bound enzymes fall on a single correlation line in the ν_{Fe-CO} versus ν_{C-O} plot (*21*). In contrast, the gsNOS data reported here demonstrate a more global conformational heterogeneity of the substrate-free enzyme, as the two $\nu_{Fe-CO}-\nu_{CO}$ data points fall on two distinct correlation lines, indicating differences on both the proximal and distal sides of the heme in the two conformers (Figure 5). Furthermore, substrate binding in gsNOS not only introduces a positive electrostatic potential into the distal heme environment but also modulates the proximal Fe−Cys bond strength, as the Raman data indicate that the Fe−Cys bond in the NOHA-bound derivative is stronger than that in the L-Arg-bound enzyme. The transduction of the distal structural signal to the proximal side is plausibly mediated by the Trp70 residue, which π-stacks with the heme and donates a H-bond to the Cys, as discussed above. It is noteworthy that in P450cam, the binding of putidaredoxin has also been shown to change the strength of the proximal Fe−Cys bond, due to the modulation of its electrostatic environment (*46*).

Although the exact mechanism for the substrate binding-induced perturbation in the proximal Fe−Cys moiety in gsNOS remains to be further investigated, the data reported here support mechanistic differences between the two steps of the NOS reaction in this bacterial enzyme. As such, it

Scheme 2

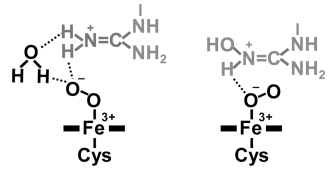

offers insights into the role of the proximal Cys → Fe electron donation in the oxygen chemistry of NOS. As illustrated in Scheme 2, one important factor leading to the two different mechanisms is that, in the L-Arg-bound enzyme, it is the terminal oxygen atom of the heme-bound dioxygen that accepts H-bonds from the substrate (L-Arg) and a water molecule, whereas in the NOHA-bound enzyme, it is the proximal oxygen atom that accepts the H-bond from the substrate (NOHA) (*32, 36, 37*). The H-bonding to the distal oxygen atom in the L-Arg-bound enzyme facilitates O−O bond cleavage, leading to the formation of the ferryl species that converts L-Arg to NOHA. In contrast, in the NOHA-bound enzyme, the H-bond donating from NOHA to the proximal oxygen atom inhibits O−O bond cleavage; instead, it stabilizes the peroxyl species that inserts itself into NOHA via a nucleophilic addition reaction to generate citrulline and NO. The stronger Fe−Cys bond in the NOHA-bound derivative, compared to that in the L-Arg-bound enzyme, revealed by the Raman data presented here indicates that the proximal Cys → Fe electron donation is stronger in the NOHA-bound enzyme. The increased "electronic push" from the proximal Cys ligand through the iron to the proximal oxygen atom plausibly strengthens its H-bond with NOHA, facilitating the second step of the NOS reaction.

CONCLUSIONS

We have shown that the CO-bound gsNOS from the thermophilic bacterium *G. stearothermophilus* exhibits two conformations in the absence of substrate, one with a stronger proximal Fe−Cys bond than the other. L-Arg stabilizes the conformer with the weaker Fe−Cys bond, whereas NOHA stabilizes the conformer with the stronger Fe−Cys bond, although both substrates introduce a positive electrostatic potential into the distal ligand binding site. The data indicate that substrate binding in the distal pocket of gsNOS modulates both the distal and proximal heme environment, in contrast to mNOS, in which only the distal properties are affected. The unique modifications in the heme active site introduced by each substrate may be critical in defining the chemical environment required for carrying out the mechanistically distinct oxygen chemistry in each step of the NOS reaction.

SUPPORTING INFORMATION AVAILABLE

Absence of significant differences resulting from the addition of H4B in the optical spectra (Figure 1S), resonance Raman spectra of the CO adducts (Figure 2S), and resonance Raman spectra of the Fe−Cys stretching mode (Figure 3S). This material is available free of charge via the Internet at http://pubs.acs.org.

REFERENCES

1. Stuehr, D. J. (1999) Mammalian nitric oxide synthases. *Biochim. Biophys. Acta 1411*, 217–230.
2. Siddhanta, U., Presta, A., Fan, B., Wolan, D., Rousseau, D. L., and Stuehr, D. J. (1998) Domain swapping in inducible nitric-oxide synthase. Electron transfer occurs between flavin and heme groups located on adjacent subunits in the dimer. *J. Biol. Chem. 273*, 18950–18958.
3. Panda, K., Ghosh, S., and Stuehr, D. J. (2001) Calmodulin activates intersubunit electron transfer in the neuronal nitric-oxide synthase dimer. *J. Biol. Chem. 276*, 23349–23356.
4. Crane, B. R., Arvai, A. S., Gachhui, R., Wu, C., Ghosh, D. K., Getzoff, E. D., Stuehr, D. J., and Tainer, J. A. (1997) The structure of nitric oxide synthase oxygenase domain and inhibitor complexes. *Science 278*, 425–431.
5. Crane, B. R., Arvai, A. S., Ghosh, D. K., Wu, C., Getzoff, E. D., Stuehr, D. J., and Tainer, J. A. (1998) Structure of nitric oxide synthase oxygenase dimer with pterin and substrate. *Science 279*, 2121–2126.
6. Raman, C. S., Li, H., Martasek, P., Kral, V., Masters, B. S., and Poulos, T. L. (1998) Crystal Structure of Constitutive Endothelial Nitric Oxide Synthase A Paradigm for Pterin Function Involving a Novel Metal Center. *Cell 95*, 939–950.
7. Li, H., Raman, C. S., Glaser, C. B., Blasko, E., Young, T. A., Parkinson, J. F., Whitlow, M., and Poulos, T. L. (1999) Crystal structures of zinc-free and -bound heme domain of human inducible nitric-oxide synthase. Implications for dimer stability and comparison with endothelial nitric-oxide synthase. *J. Biol. Chem. 274*, 21276–21284.
8. Li, H., Shimizu, H., Flinspach, M., Jamal, J., Yang, W., Xian, M., Cai, T., Wen, E. Z., Jia, Q., Wang, P. G., and Poulos, T. L. (2002) The novel binding mode of N-alkyl-N′-hydroxyguanidine to neuronal nitric oxide synthase provides mechanistic insights into NO biosynthesis. *Biochemistry 41*, 13868–13875.
9. Fedorov, R., Hartmann, E., Ghosh, D. K., and Schlichting, I. (2003) Structural basis for the specificity of the nitric-oxide synthase inhibitors W1400 and Nω-propyl-L-Arg for the inducible and neuronal isoforms. *J. Biol. Chem. 278*, 45818–45825.
10. Chen, P. F., Tsai, A. L., Berka, V., and Wu, K. K. (1996) Endothelial nitric-oxide synthase. Evidence for bidomain structure and successful reconstitution of catalytic activity from two separate domains generated by a baculovirus expression system. *J. Biol. Chem. 271*, 14631–14635.
11. Wang, J., Stuehr, D. J., Ikeda-Saito, M., and Rousseau, D. L. (1993) Heme coordination and structure of the catalytic site in nitric oxide synthase. *J. Biol. Chem. 268*, 22255–22258.
12. Wang, J., Stuehr, D. J., and Rousseau, D. L. (1995) Tetrahydrobiopterin-deficient nitric oxide synthase has a modified heme environment and forms a cytochrome P-420 analogue. *Biochemistry 34*, 7080–7087.
13. Wang, J., Stuehr, D. J., and Rousseau, D. L. (1997) Interactions between substrate analogues and heme ligands in nitric oxide synthase. *Biochemistry 36*, 4595–4606.
14. Fan, B., Wang, J., Stuehr, D. J., and Rousseau, D. L. (1997) NO synthase isozymes have distinct substrate binding sites. *Biochemistry 36*, 12660–12665.
15. Tierney, D. L., Martasek, P., Doan, P. E., Masters, B. S. S., and Hoffman, B. M. (1998) Location of guanidino nitrogen of L-arginine substrate bound to neuronal nitric oxide synthase (nNOS): Determination by Q-band ENDOR spectroscopy. *J. Am. Chem. Soc. 120*, 2983–2984.
16. Couture, M., Adak, S., Stuehr, D. J., and Rousseau, D. L. (2001) Regulation of the properties of the heme-NO complexes in nitric-oxide synthase by hydrogen bonding to the proximal cysteine. *J. Biol. Chem. 276*, 38280–38288.
17. Adak, S., Crooks, C., Wang, Q., Crane, B. R., Tainer, J. A., Getzoff, E. D., and Stuehr, D. J. (1999) Tryptophan 409 controls the activity of neuronal nitric-oxide synthase by regulating nitric oxide feedback inhibition. *J. Biol. Chem. 274*, 26907–26911.
18. Adak, S., Wang, Q., and Stuehr, D. J. (2000) Molecular basis for hyperactivity in tryptophan 409 mutants of neuronal NO synthase. *J. Biol. Chem. 275*, 17434–17439.
19. Adak, S., and Stuehr, D. J. (2001) A proximal tryptophan in NO synthase controls activity by a novel mechanism. *J. Inorg. Biochem. 83*, 301–308.
20. Voegtle, H. L., Sono, M., Adak, S., Pond, A. E., Tomita, T., Perera, R., Goodin, D. B., Ikeda-Saito, M., Stuehr, D. J., and Dawson, J. H. (2003) Spectroscopic characterization of five- and six-coordinate ferrous-NO heme complexes. Evidence for heme Fe-proximal cysteinate bond cleavage in the ferrous-NO adducts of the Trp-409Tyr/Phe proximal environment mutants of neuronal nitric oxide synthase. *Biochemistry 42*, 2475–2484.

21. Rousseau, D. L., Li, D., Couture, M., and Yeh, S. R. (2005) Ligand-protein interactions in nitric oxide synthase. *J. Inorg. Biochem. 99*, 306–323.
22. Kers, J. A., Wach, M. J., Krasnoff, S. B., Widom, J., Cameron, K. D., Bukhalid, R. A., Gibson, D. M., Crane, B. R., and Loria, R. (2004) Nitration of a peptide phytotoxin by bacterial nitric oxide synthase. *Nature 429*, 79–82.
23. Chen, Y., and Rosazza, J. P. (1995) Purification and characterization of nitric oxide synthase (NOSNoc) from a *Nocardia* species. *J. Bacteriol. 177*, 5122–5128.
24. Buddha, M. R., Keery, K. M., and Crane, B. R. (2004) An unusual tryptophanyl tRNA synthetase interacts with nitric oxide synthase in *Deinococcus radiodurans*. *Proc. Natl. Acad. Sci. U.S.A. 101*, 15881–15886.
25. Santolini, J., Roman, M., Steuhr, D. J., and Mattioli, T. A. (2006) Resonance Raman Study of *Bacillus subtilis* NO synthase-like protein: Similarities and differences with mammalian NO synthases. *Biochemistry 45*, 1489–1489.
26. Salard, I., Mercey, E., Rekka, E., Boucher, J. L., Nioche, P., Mikula, I., Martasek, P., Raman, C. S., and Mansuy, D. (2006) Analogies and surprising differences between recombinant nitric oxide synthase-like proteins from *Staphylococcus aureus* and *Bacillus anthracis* in their interactions with L-arginine analogs and iron ligands. *J. Inorg. Biochem. 100*, 2024–2033.
27. Chartier, F. J., and Couture, M. (2004) Stability of the heme environment of the nitric oxide synthase from *Staphylococcus aureus* in the absence of pterin cofactor. *Biophys. J. 87*, 1939–1950.
28. Sudhamsu, J., and Crane, B. R. (2006) Structure and reactivity of a thermostable prokaryotic nitric-oxide synthase that forms a long-lived oxy-heme complex. *J. Biol. Chem. 281*, 9623–9632.
29. Pant, K., Bilwes, A. M., Adak, S., Stuehr, D. J., and Crane, B. R. (2002) Structure of a nitric oxide synthase heme protein from *Bacillus subtilis*. *Biochemistry 41*, 11071–11079.
30. Bird, L. E., Ren, J., Zhang, J., Foxwell, N., Hawkins, A. R., Charles, I. G., and Stammers, D. K. (2002) Crystal Structure of SANOS, a Bacterial Nitric Oxide Synthase Oxygenase Protein from *Staphylococcus aureus*. *Structure 10*, 1687–1696.
31. Crane, B. R., Rosenfeld, R. J., Arvai, A. S., Ghosh, D. K., Ghosh, S., Tainer, J. A., Stuehr, D. J., and Getzoff, E. D. (1999) N-Terminal domain swapping and metal ion binding in nitric oxide synthase dimerization. *EMBO J. 18*, 6271–6281.
32. Li, D., Kabir, M., Stuehr, D. J., Rousseau, D. L., and Yeh, S. R. (2007) Substrate- and isoform-specific dioxygen complexes of nitric oxide synthase. *J. Am. Chem. Soc. 129*, 6943–6951.
33. Rousseau, D. L., Li, D., Hayden, E. Y., Deng, H., and Yeh, S. R. (2008) Ligand-Protein Interactions in Mammalian Nitric Oxide Synthase. In *The Smallest Biomolecules: Diatomics and their Interactions with Hemeproteins* (Ghosh, A., Ed.) pp 465−497, Elsevier, Amsterdam.
34. Griffith, O. W., and Stuehr, D. J. (1995) Nitric oxide synthases: properties and catalytic mechanism. *Annu. Rev. Physiol. 57*, 707–736.
35. Pufahl, R. A., Wishnok, J. S., and Marletta, M. A. (1995) Hydrogen peroxide-supported oxidation of NG-hydroxy-L-arginine by nitric oxide synthase. *Biochemistry 34*, 1930–1941.
36. Li, H., Igarashi, J., Jamal, J., Yang, W., and Poulos, T. L. (2006) Structural studies of constitutive nitric oxide synthases with diatomic ligands bound. *J. Biol. Inorg. Chem. 11*, 753–768.
37. Pant, K., and Crane, B. R. (2006) Nitrosyl-heme structures of *Bacillus subtilis* nitric oxide synthase have implications for understanding substrate oxidation. *Biochemistry 45*, 2537–2544.
38. Li, D., Stuehr, D. J., Yeh, S. R., and Rousseau, D. L. (2004) Heme distortion modulated by ligand-protein interactions in inducible nitric-oxide synthase. *J. Biol. Chem. 279*, 26489–26499.
39. Rousseau, D. L., Li, D., Couture, M., and Yeh, S. R. (2005) Ligand-protein interactions in nitric oxide synthase. *J. Inorg. Biochem. 99*, 306–323.
40. Yu, N.-T., and Kerr, E. A. (1987) in *Biological Applications of Raman Spectroscopy: Resonance Raman Spectra of Hemes and Metalloproteins* (Spiro, T. G., Ed.) pp 39−96, Wiley, New York.
41. Egawa, T., and Yeh, S. R. (2005) Structural and functional properties of hemoglobins from unicellular organisms as revealed by resonance Raman spectroscopy. *J. Inorg. Biochem. 99*, 72–96.
42. Spiro, T. G., and Wasbotten, I. H. (2005) CO as a vibrational probe of heme protein active sites. *J. Inorg. Biochem. 99*, 34–44.
43. Xu, C., Ibrahim, M., and Spiro, T. G. (2008) DFT analysis of axial and equatorial effects on heme-CO vibrational modes: Applications to CooA and H-NOX heme sensor proteins. *Biochemistry 47*, 2379–2387.
44. Bangcharoenpaurpong, O., Champion, P. M., Martinis, S. A., and Sligar, S. G. (1987) Investigations of the resonance Raman excitation profiles of cytochrome $P450_{cam}$. *J. Chem. Phys. 87*, 4273–4284.
45. Champion, P. M., Stallard, B. R., Wagner, G. C., and Gunsalus, I. C. (1982) Resonance Raman detection of an iron-sulfur bond in cytochrome P450cam. *J. Am. Chem. Soc. 104*, 5469–5472.
46. Unno, M., Christian, J. F., Sjodin, T., Benson, D. E., Macdonald, I. D., Sligar, S. G., and Champion, P. M. (2002) Complex formation of cytochrome P450cam with putidaredoxin. Evidence for protein-specific interactions involving the proximal thiolate ligand. *J. Biol. Chem. 277*, 2547–2553.
47. Schelvis, J. P., Berka, V., Babcock, G. T., and Tsai, A. L. (2002) Resonance Raman detection of the Fe-S bond in endothelial nitric oxide synthase. *Biochemistry 41*, 5695–5701.
48. Dawson, J. H. (1988) Probing structure-function relations in heme-containing oxygenases and peroxidases. *Science 240*, 433–439.
49. Pant, K., and Crane, B. R. (2005) Structure of a loose dimer: An intermediate in nitric oxide synthase assembly. *J. Mol. Biol. 352*, 932–940.
50. Couture, M., Stuehr, D. J., and Rousseau, D. L. (2000) The ferrous dioxygen complex of the oxygenase domain of neuronal nitric-oxide synthase. *J. Biol. Chem. 275*, 3201–3205.
51. Unno, M., Christian, J. F., Benson, D. E., Gerber, N. C., Sligar, S. G., and Champion, P. M. (1997) Resonance Raman Investigations of Cytochrome P450cam Complexed with Putidaredoxin. *J. Am. Chem. Soc. 119*, 6614–6620.

BI801491E